Investigation of the separation bubble formed behind the sharp leading edge of a flat plate at incidence

M J Crompton and **R V Barrett***
Department of Aerospace Engineering, University of Bristol, Queen's Building, UK

Abstract: Detailed measurements of the separation bubble formed behind the sharp leading edge of a flat plate at low speeds and incidence are reported. The Reynolds number based on chord length ranged from 0.1×10^5 to 5.5×10^5.

Extensive use of laser Doppler anemometry allowed detailed velocity measurements throughout the bubble. The particular advantages of laser Doppler anemometry in this application were its ability to define flow direction without ambiguity and its non-intrusiveness. It allowed the mean reattachment point to be accurately determined. The static pressure distribution along the plate was also measured.

The length of the separation bubble was primarily determined by the plate incidence, although small variations occurred with Reynolds number because of its influence on the rate of entrainment and growth of the shear layer. Above about 10^5, this Reynolds number effect was no longer evident.

The reverse flow boundary layer in the bubble exhibited signs of periodic stabilization before separating close to the leading edge, forming a small secondary bubble rotating in the opposite sense to the main bubble.

Keywords: sharp leading edge, separation bubble, flat plate, laser Doppler anemometer, separation, reattachment, shear layer

NOTATION

c	chord length
C_p	pressure coefficient $= (p - p_\infty)/(\frac{1}{2}\rho U_\infty^2)$
p	static pressure
Re_c	Reynolds number based on chord length
u	local chordwise fluid velocity
$u_{r.m.s.}$	root mean square component of chordwise fluid velocity
U_∞	freestream fluid velocity
x	chordwise distance from leading edge
x_R	separation bubble reattachment length
y	distance normal to surface
α	angle of incidence
ρ	density
σ	pressure recovery factor

Subscripts

∞	freestream conditions
R	reattachment
S	separation

The MS was received on 26 January 2000 and was accepted after revision for publication on 8 June 2000.
**Corresponding author: Department of Aerospace Engineering, University of Bristol, Queen's Building, University Walk, Bristol BS8 1TR, UK.*

1 INTRODUCTION

Separation bubbles may occur on the rounded surfaces of conventional aerofoils and also, in a different form, off the sharp leading edges of thin aerofoils and membranes. Most previous research has concentrated on the short separation bubble that occurs in the former case. This type of bubble is characterized by a laminar separation followed by rapid transition and reattachment. Under normal flight conditions, such bubbles occur near the leading edge, but at low Reynolds number they may be situated well aft on the aerofoil. The bubble, although rapidly curtailed, will influence aerofoil performance, leading to premature stall on bursting. In certain circumstances the burst bubble will reattach further along the aerofoil before finally detaching from the surface. In this situation it takes on the long bubble form that is the subject of this paper. More

typically, long bubbles form as a result of separation on thin aerofoils at a sharp leading edge. This type of bubble has received somewhat less attention than the short bubble. It became of interest in the 1950s with the move to higher flight speeds and the consequent need for the use of thin aerofoils to reduce compressibility effects. Interest was heightened further by developments in turbomachinery towards thinner, more efficient blading and by the increasing drive to understand the characteristics of thin flexible aerofoils in sailing and in low Reynolds number aviation activities. The separation bubble from a sharp or small radius leading edge is characterized by a fixed separation process resulting from the unsustainable pressure gradient at the leading edge and by delayed reattachment, the bubble length increasing with incidence. The nature of the bubble bears closer relation to the separation behind steps, fences and similar obstacles than to the short bubble on a rounded aerofoil. This is in line with the findings of Castro and Haque [**1**] who argued that for a wide range of complex turbulent flows, in which an extensive recirculation region is bounded by a shear layer, the general features are likely to be similar.

The investigation described considers the most basic case of the leading edge bubble, i.e. that formed over a two-dimensional thin flat plate at incidence with a sharp leading edge in incompressible flow. This has been identified as an important test case in the development of numerical calculations for thin aerofoils, for example as cited by Jackson and Fiddes [**2**] in a study of flexible sail membranes. As well as providing direct data, the objective was to provide further understanding of the flow phenomenon which was seen to be incomplete from previous work. To do this, laser Doppler anemometry was used, thus eliminating problems of directional ambiguity and probe interference that had previously been a limitation when measuring in the separation bubble, using, for example, hot-wire methods. With the laser Doppler anemometer (LDA), detailed measurements of mean and fluctuating components of velocity were obtained within and downstream of the bubble, taking particular advantage of its high spatial resolution and small measurement volume to define precisely the steep velocity gradients and small-scale flow features contained within the bubble. The results reveal previously unexplored small-scale flow features and provide data that should be of value in the development and validation of numerical simulations for thin aerofoil separation bubbles.

2 EXPERIMENTAL METHOD

2.1 Wind tunnel rig and instrumentation

Tests were carried out on a series of two-dimensional flat plates of various chord lengths and over a range of Reynolds number, Re_c, of 0.2×10^5–5.5×10^5. All were chamfered at 20° on the lower surface to produce a sharp leading edge and had a thickness–chord ratio of 3.75 per cent. A plate of 160 mm chord was used for the majority of the tests. This was provided with pressure tappings at a position offset from the centre-line where the velocity measurements were made.

The plates were mounted horizontally in the University of Bristol low-turbulence wind tunnel [**3**]. This is a closed-loop design with internal working section dimensions of 0.8 m × 0.6 m × 1.6 m (width × height × length) and a freestream turbulence intensity below 0.05 per cent for the range of speeds used in this investigation, i.e. up to 40 m/s. To reduce end effects, the plates were sealed against the side walls of the tunnel, although no attempt was made to remove the wall boundary layer. A survey into flow three-dimensionality showed the bubble reattachment distance to remain constant over the central 60 per cent of the plate for an incidence of 3°. Thus, end effects are not eliminated, but a central region of planar flow normal to the spanwise axis is achieved to give effectively two-dimensional conditions in this region. Corrections to the incidence should strictly be applied to account for the influence of three-dimensional effects outside this region as well as for the general effects of wind tunnel interference. Estimates of these corrections showed them to be sufficiently small to be ignored for the general analysis of the results given herein. Although the use of large end plates has been shown previously to give a greater proportion of planar flow in similar experiments [**4**], this approach would not have been so readily compatible with the use of laser anemometry.

The flow was examined mainly through surface pressure and velocity measurement, the latter using a Dantec three-component, fibre optic-coupled LDA which enabled full, mean and time-varying velocity data to be taken for three mutually perpendicular axes in a manner non-intrusive to the flow. The projection optics, of 600 mm focal length, were mounted outside the tunnel on a precision three-axis traversing rig with operating dimensions of 0.6 m × 0.6 m × 0.6 m. This, together with other aspects of the data acquisition process, was controlled through a computer. The system, as described by Barrett and Swales [**5**], was configured to run in off-axis backscatter mode in order to achieve the smallest possible measurement volume, this being of the order of 0.05 mm in diameter and near spherical. Seeding was provided by a Safex 2001 fogger using a glycol-based fluid. It produces a uniform distribution of particles with an average diameter of 1 μm.

2.2 Measurement errors

The enhanced alignment methods developed at Bristol University [**5**] allow routine operation in the off-axis

mode while maintaining high data rates. As a consequence, a minimization of errors is achieved owing to the greatly reduced effective measurement volume. This allows:

(a) precise three-dimensional measurement in poorly seeded areas while maintaining satisfactory data rates;
(b) increased positional accuracy in defining the location of the surface and for velocity measurements in the boundary layer close to the surface (< 0.1 mm);
(c) reduced statistical errors in regions of high velocity gradient.

For the current work, the quasi-two-dimensional nature of the flow in which the velocity is predominantly in the streamwise direction reduces some error sources considerably. The general accuracy of the system when aligned by the method described and configured to run in off-axis mode was analysed by MacManus *et al.* [**6**], based on tests carried out at Bristol University using the same LDA system.

The main errors associated with the LDA in the present application can be categorized as:

1. *Seeding particle behaviour*. For particles with a mean diameter of around 1 μm, flow accelerations can be shown to cause negligible deviation in particle path relative to the flow direction and therefore small errors in velocity. For example, Melling and Whitelaw [**7**] found the largest errors due to the effects in a vortex core to be of the order of 0.007 m/s in the radial component, equating to an error in total velocity of < 0.01 per cent. In the present study, the flow contains no vortex regions as strong as this and therefore the centripetal influence will be negligible.
2. *Frequency measurement errors*. The processors determine the Doppler frequency by Fourier analysis of the signal, employing a high discretization resolution, resulting in a maximum error of < 0.001 m/s for each velocity component measured.
3. *Calibration and transformation errors*. The frequencies are converted to velocities and transformed into the desired axis system using a velocity transformation matrix. In general, the accuracy in determining this matrix is of the order of the positional accuracy of the traverse (± 0.02 mm). The beam orientations were chosen to minimize the errors in the plane of the two-dimensional flow, which were calculated to be within the range 0.1–0.8 per cent, depending on the local flow velocities. The out-of-plane errors were greater than this but were of little consequence to the results presented.
4. *Statistical errors*. These occur owing to:

   (a) *Finite sample size*. Errors occur because of the finite sample size recorded in relation to the overall unsteadiness of the flow. Following the approach of Pfeifer [**8**], it was calculated that, for a measurement obtained from 5000 samples, the maximum errors were ± 0.007 m/s (mean velocity) and ± 0.023 m/s [root mean square (r.m.s.)] in the region of flow with the highest turbulence intensity, for a confidence limit of 95 per cent.
   (b) *Velocity bias*. In a fluctuating flow, a greater proportion of particles pass through the measurement volume at times when the velocity is high than when it is low. Therefore, a bias of the mean velocity is recorded that is dependent on the turbulence intensity. For the flow under investigation, this was found to be of the order of 0.0002 m/s, based on an analysis given by McLaughlin and Tiedermann [**9**].
   (c) *Gradient bias*. When a velocity gradient exists across the diameter of the measurement volume, more particles pass through the higher velocity region, thereby biasing the measured mean velocity. In the present study, this effect is most significant in the shear layer close to the leading edge where the highest velocity gradient occurs (40 m/s per mm), giving a maximum bias of 0.052 m/s.

5. *Positional accuracy*. The greatest positional error was in the determination of the location of the surface of the plate. By monitoring the output of the photomultiplier anode current as the measurement volume was traversed towards the surface, the uncertainty was reduced to the resolution of the traverse, i.e. ±0.005mm in the vertical direction. Based on the same maximum velocity gradient as quoted earlier, this equates to a maximum error of ± 0.200 m/s.

Most of the statistical errors are variable over the flowfield and small relative to the freestream velocity and are therefore only important in local regions of steep velocity gradient or high velocity fluctuation. The interdependent nature of various errors makes any estimate of the overall error difficult to ascertain. Maximum errors in mean velocity range from the order of 0.5 per cent in the freestream areas to < 2 per cent in local regions of steep velocity gradients.

3 DISCUSSION

3.1 General bubble structure

The general flow structure of a typical leading edge separation bubble on a flat plate with a sharp leading edge can be seen by the contour plots of mean and r.m.s. chordwise velocity components shown respectively in Figs 1 and 2, normalized to the freestream tunnel

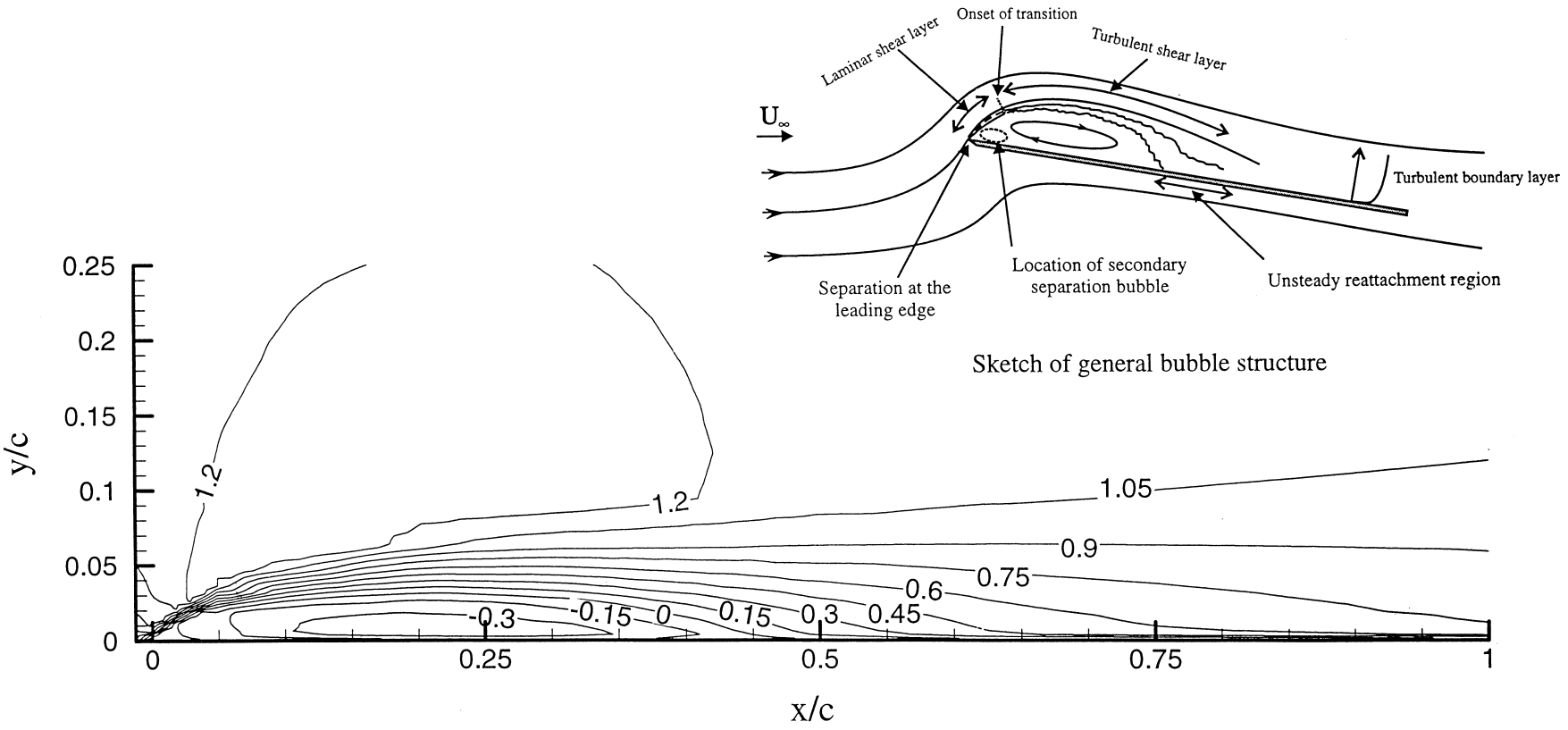

Fig. 1 Mean chordwise velocity u/U_∞ for $\alpha = 3°$, $U_\infty = 20\,\text{m/s}$ and $Re_c = 2.13 \times 10^5$

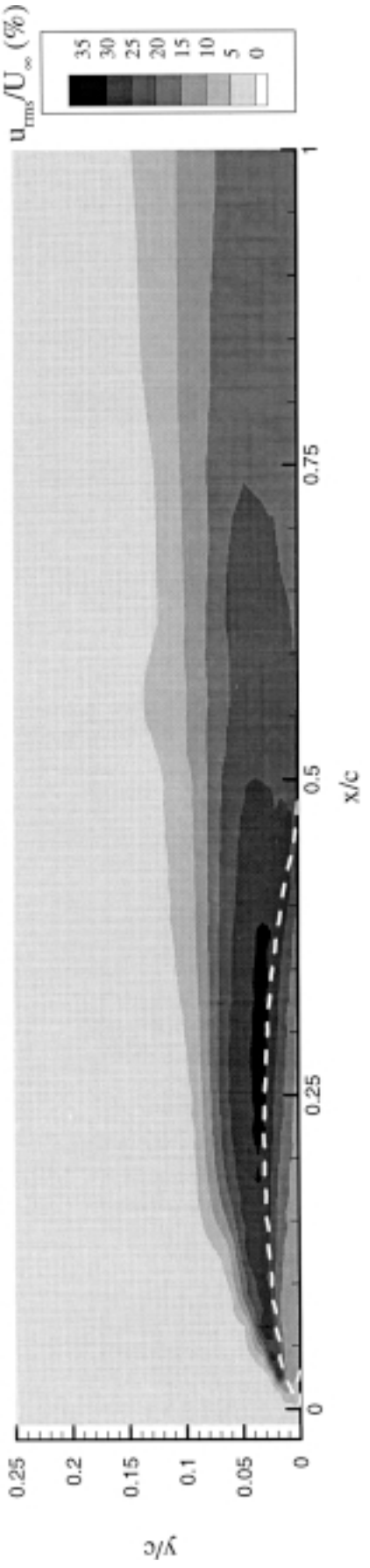

Fig. 2 Chordwise r.m.s. velocity $u_{\text{r.m.s.}}/U_\infty$ for $\alpha = 3^\circ$, $U_\infty = 20\,\text{m/s}$ and $Re_c = 2.13 \times 10^5$: – – – locus of $u/U_\infty = 0$

speed U_∞. A sketch of the flow structure is also included in Fig. 1. The example is for a Reynolds number of 2.13×10^5, with a plate incidence of 3°, producing a reattachment length of $x_R/c = 0.47$. The reattachment point is defined as the location along the chord at which the mean chordwise velocity gradient at the surface is zero. This was interpreted for practical purposes in the present work as the position with zero mean chordwise velocity at the closest measurement location to the surface attainable, i.e. 0.05 mm. The reattachment region is highly unstable, it is therefore essential that an instrument able properly to resolve flow reversal, such as the LDA, is used.

The shear layer can be seen to thicken at a low rate up to about 5 per cent chord from the leading edge where a substantially increased rate of thickening begins, as indicated by a widening of the mean velocity contours. The increase is due to transition of the shear layer from a laminar to a turbulent state. The associated increase in turbulence is seen to begin a little closer to the leading edge than 5 per cent chord. Turbulence intensity reaches a peak close to the maximum thickness of the bubble, before decreasing as the shear layer bends towards the surface and reattaches. After reattachment, the reduction in turbulence intensity continues to the trailing edge owing to the relaxation of the new attached boundary layer, as noted previously by Bradshaw and Wong [**10**]. The reason why the reduction in turbulence intensity begins before reattachment is twofold:

1. In the general downflow near reattachment, eddies approaching the surface will be damped out.
2. The bifurcation of the shear layer will tend to split large eddies into smaller ones.

Supporting this, Bradshaw and Wong measured a rapid decrease in the turbulent shear stress and eddy length scale just downstream of reattachment.

The strong reverse flow component of the separation bubble reaches a maximum mean velocity of $0.4U_\infty$, the fluid being driven by the entrainment process provided by the shear layer. It is particularly energetic because most of the shear layer, i.e. at least 95 per cent is turbulent. This contrasts with short separation bubbles on rounded aerofoils where a considerable portion of the shear layer, sometimes as much as 80 per cent of the length, is laminar [**11**]), and the maximum reverse flow velocity is typically less than $0.2U_\infty$.

Over the front portion of the bubble, the outer flow is subject to a large acceleration, similar to that experienced around a conventional rounded aerofoil. For an incidence of 3°, the velocity reaches a maximum value of $1.3U_\infty$ at 20 per cent bubble length, and it is this acceleration and hence the low values of static pressure reached that provide the main source of lift on the flat plate.

Castro and Haque [**1**] first highlighted evidence suggesting that the boundary layer in the reverse flow region can develop 'laminar-like' features, in an experiment where separation was induced by a small plate normal to the flow with reattachment on a downstream central splitter plate. This effect is indicated in Fig. 2, which shows a noticeable drop in turbulence intensity as the reverse flow progresses, suggesting that the boundary layer is stabilizing. Figure 3 shows detailed mean chordwise velocity profiles perpendicular to the surface at various distances downstream, while Fig. 4 shows the chordwise r.m.s. velocity for the same locations. An enlarged view of the part of the mean velocity profiles in the reverse flow (see inset, Fig. 3) shows a reduction in the velocity gradient near the surface as the flow meets the adverse pressure gradient along the forward part of the bubble. This leaves the boundary layer more susceptible to separation.

The velocity profiles before reattachment show very steep gradients across the shear layer, above which the velocity peaks and then tails off gradually in the freestream. The location of the steepest velocity gradient coincides with maximum turbulence intensity. Profiles after reattachment show how the boundary layer relaxes, tending towards a normal turbulent profile.

At reattachment, the velocity profile displays a form unique to reattaching turbulent shear layers, with an almost linear region from close to the surface to the edge of the boundary layer. Horton [**12**] identified the similarity in many such profiles by analysing existing data from which he proposed a universal reattachment profile based on a semi-empirical method of analysis. The resulting shape had a zero velocity gradient at the wall, a necessary parameter for flow reattachment, followed by a constant gradient near to the edge of the boundary layer. Schmidt and Mueller [**13**] used results by O'Meara [**14**] for comparison with Horton's universal profile. O'Meara's profiles were obtained very close to his estimate of the reattachment point but were much fuller in shape than Horton's universal profile would suggest, with higher velocities near the wall and no obvious tendency towards a zero slope. Schmidt and Mueller attributed the difference either to the measurement location being further downstream of reattachment than estimated or to distortion of the profiles by the hot-wire measurement technique used. In the present study, the nearest velocity profile to reattachment was taken at approximately 3 per cent chord downstream. This profile, shown in Fig. 3, conforms generally with Horton's, but the inner region of near-zero gradient is seen to be suppressed in height, a possible consequence of the very high turbulence in this region.

Downstream, the newly attached boundary layer initially exhibits a very different profile to that of a conventional turbulent boundary layer. It consists of a region of very steep velocity gradient near the surface, almost too thin to measure, where a new inner boundary layer is developing, and, above this, a broad region of near-constant velocity gradient extends to freestream

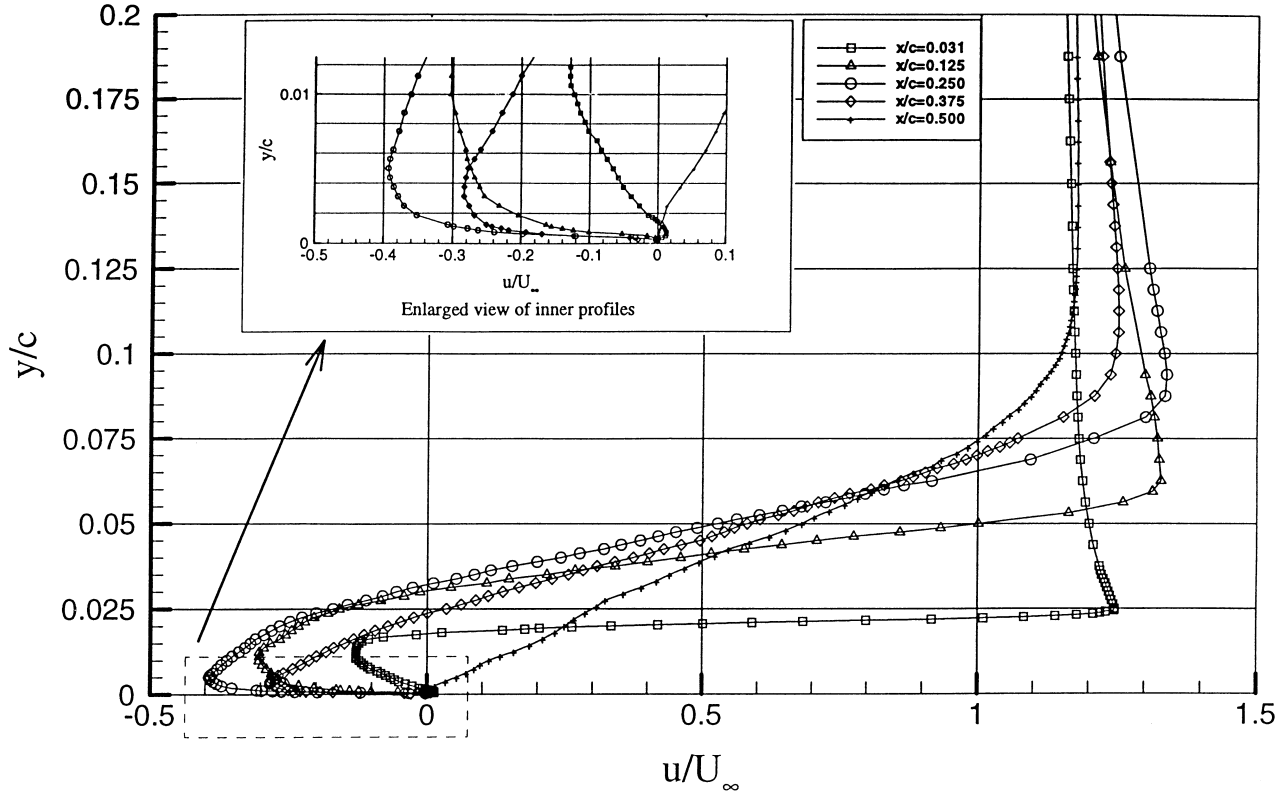

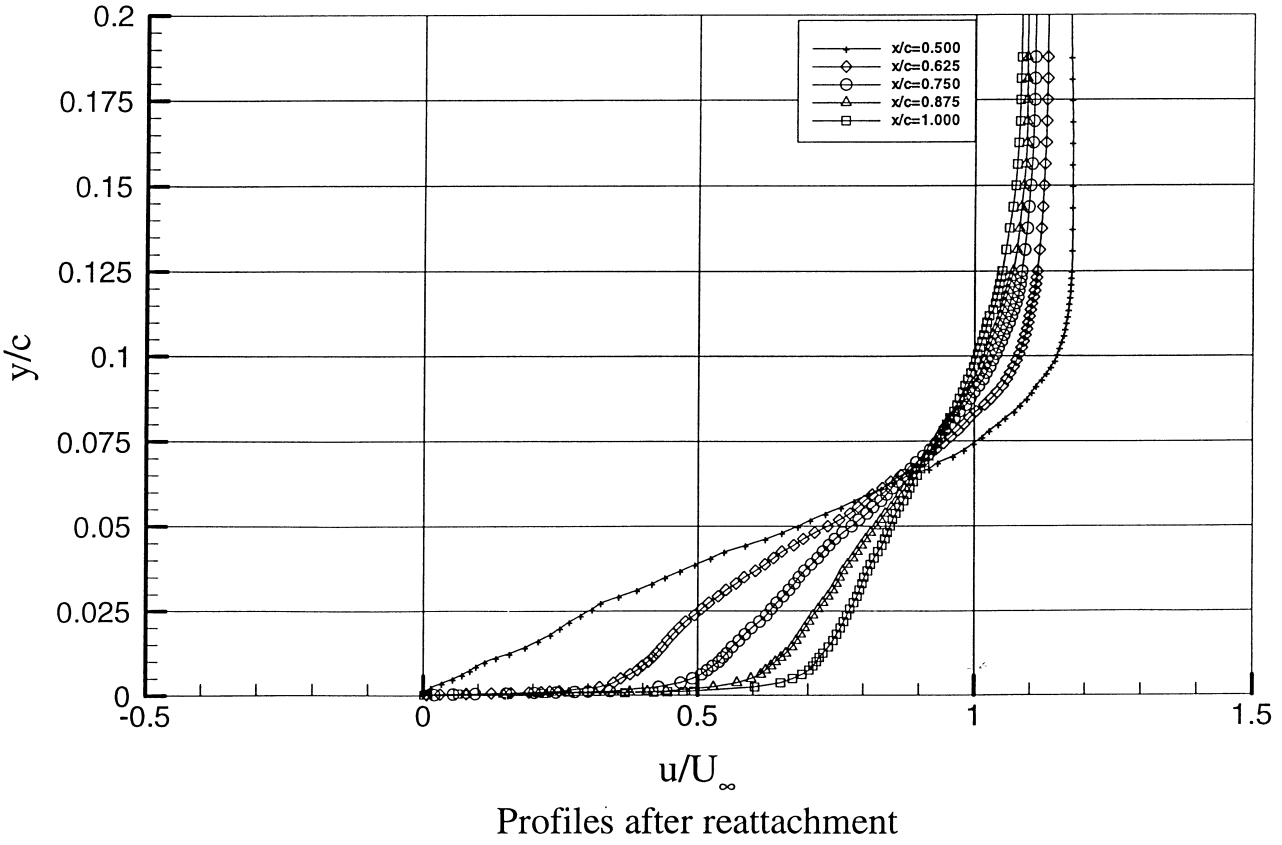

Fig. 3 Mean chordwise velocity distributions normal to the plate for $\alpha = 3°$, $U_\infty = 20\,\text{m/s}$ and $Re_c = 2.13 \times 10^5$

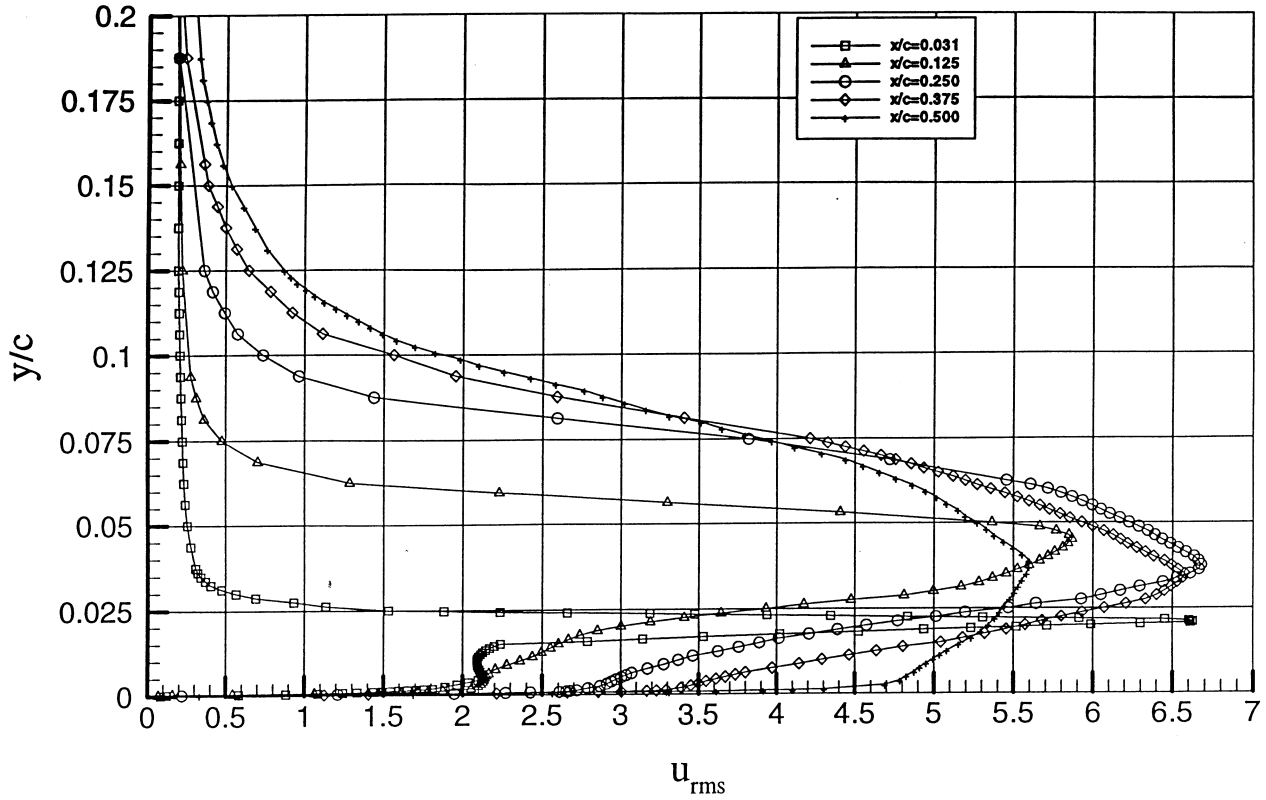

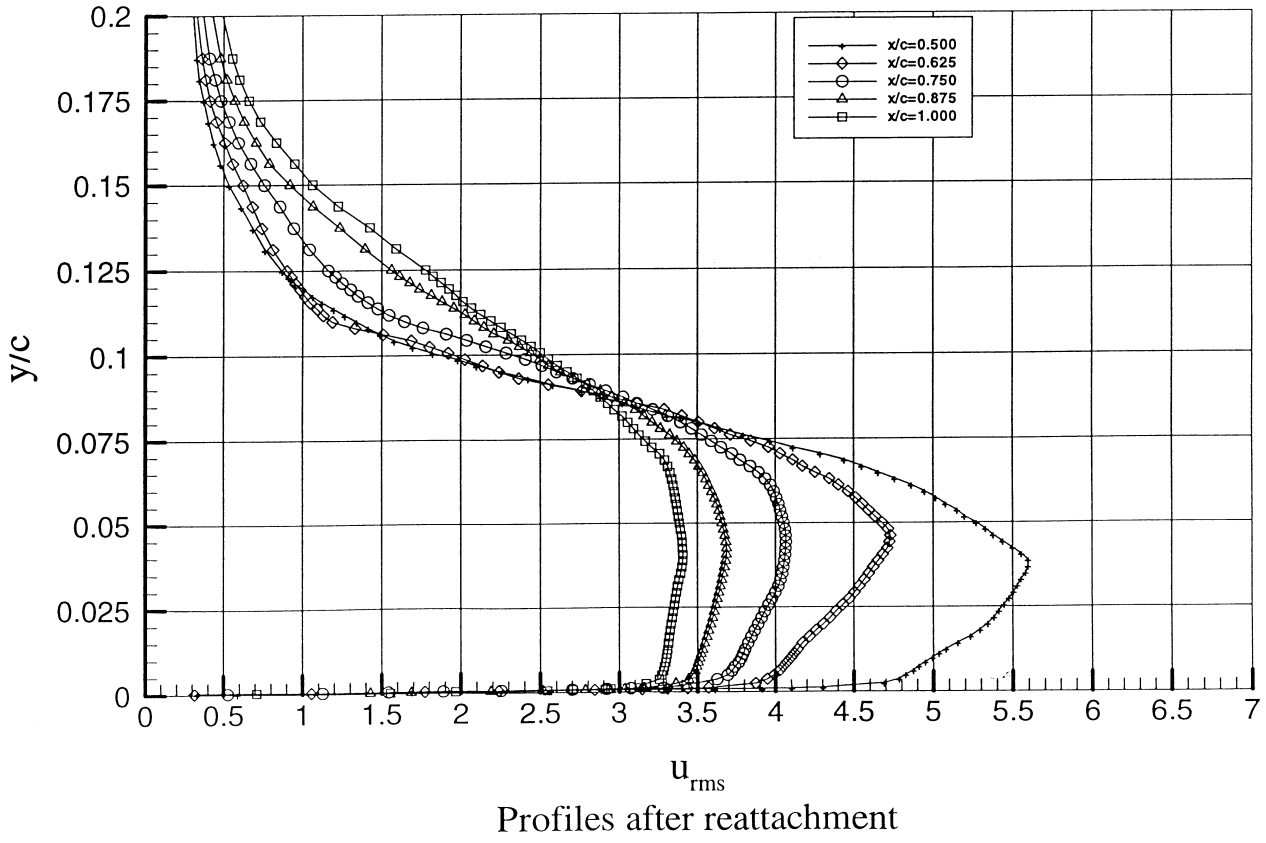

Fig. 4 Chordwise r.m.s. velocity $u_{\text{r.m.s.}}/U_\infty$ normal to the plate for $\alpha = 3°$, $U_\infty = 20$ m/s and $Re_c = 2.13 \times 10^5$

conditions. During the relaxation process the lower half of this region is accelerated by the high-energy flow being injected into it from above, but the profile retains its near-constant gradient.

Although the majority of the fluid that forms the reverse flow region is likely to come from the splitting of the shear layer in the reattachment region, fluid will also enter this region further upstream by the movement of large eddies from the shear layer towards the wall, as suggested by Simpson *et al.* [**15**]. This process is indicated by the inflections seen in the profile of chordwise r.m.s. velocity in the reverse flow region (see Fig. 4), which are caused by the conversion of the vertical velocity into components parallel to the wall as it is approached. The injection of eddies into the reverse flow region causes increased turbulence and increases chordwise intermittency.

3.2 Effects of incidence variation on the flow structure

Figure 5 shows the static pressure coefficients over the plate for angles of incidence at which the separation bubble reattaches to the surface. The minimum pressure occurs over the front portion of the bubble where there is a pressure plateau. This is followed by a region of strong pressure recovery up to and beyond reattachment, with zero pressure gradient further downstream. The maximum adverse pressure gradient exists just prior to the reattachment point and the relaxation of the turbulent boundary layer occurs mainly in zero pressure gradient. The bubble grows in length as the incidence is increased, with the shorter bubbles sustaining the stronger adverse pressure gradients. In Fig. 6 the same data are presented with the chordwise distance non-dimensionalized with respect to the reattachment length, showing the similarity in the pressure distributions.

Figure 7 shows the chordwise distribution of the intermittency of the reverse flow region measured 0.5 mm from the surface, i.e. the percentage of time that reversed flow is occurring. This is normalized with respect to the reattachment length, and again shows similarity between bubbles of different lengths. Because the measurements were taken above the surface, the reattachment point does not occur at 50 per cent reverse flow, as would be the case at the surface. If the reattachment region is defined as where there is between 5 and 95 per cent reverse flow, it is seen to occupy a length of $\pm 0.4 x_R$ for all bubble lengths. This agrees well with previous work carried out on a sudden expansion by Westphal *et al.* [**16**] who concluded that all recirculating regions bounded by turbulent shear layers were likely to be dynamically similar. In the 1° incidence case, the bubble is much shallower relative to the height of the measurement location, and Fig. 7 shows this to cause an offset towards lower intermittency in comparison with the other incidences.

As mentioned previously, the boundary layer in the reverse flow region appears to stabilize as it develops towards the leading edge. The inset time traces of velocity in Fig. 7, taken at half bubble length, show this as a periodic suppression of the turbulent fluctuations. This stabilization is associated with the favourable pressure gradient over the rear half of the bubble.

There are many differences between the long separation bubble investigated here and the short bubble, but also some similarities. The firm basis of research on short bubbles can therefore provide clues to flow mechanisms in the long bubble. Work by Crabtree [**17**] and Gaster [**18**], among others, looked at the significance of pressure gradient on the short separation bubble. They concluded that, in order to overcome the chordwise positive pressure gradient and allow the separation bubble to reattach, the shear stress had to be above a certain minimum value in the turbulent entrainment region. Crabtree defined a pressure recovery factor, σ, for the bubble that was based on the static pressure coefficients at separation and reattachment, i.e.

$$\sigma = \frac{p_R - p_S}{\frac{1}{2}\rho U_\infty^2} = \frac{C_{p_R} - C_{p_S}}{1 - C_{p_S}}$$

and showed that the maximum value above which the bubble could not be maintained and 'bursting' would occur was $\sigma \approx 0.35$. In order to calculate the values of pressure recovery factor for long bubbles in the present investigation, the minimum value of C_p was used in place of the value of C_p at separation, which cannot be determined. The result (Fig. 8) shows an almost constant value of pressure recovery factor of around 0.35 as incidence is increased, agreeing closely with analysis of the work carried out by Gault [**11**]. This is in marked contrast to the short bubble which shows a steep linear increase in pressure recovery factor with incidence, until bursting occurs, as illustrated by Crabtree's results which are also shown in Fig. 8. Because, in the case of a sharp leading edge, σ remains constant at a value close to that which causes bursting in short bubbles, it is suggested that the turbulent shear layer is maintaining close to the maximum sustainable shear stress.

3.3 Position of the stagnation point

The position of the stagnation point is expected to be dependent on incidence. However, the pressure profiles in Fig. 5 indicate that the stagnation point remains at the leading edge for all incidences at which the separation bubble reattaches. To investigate this further, LDA measurements were made on a smaller plate at a Reynolds number of 0.2×10^5 over a wide range of incidence. Figure 9 shows the results of this study. The stagnation point converges rapidly on the leading edge as incidence is reduced. By 20° incidence, the location is

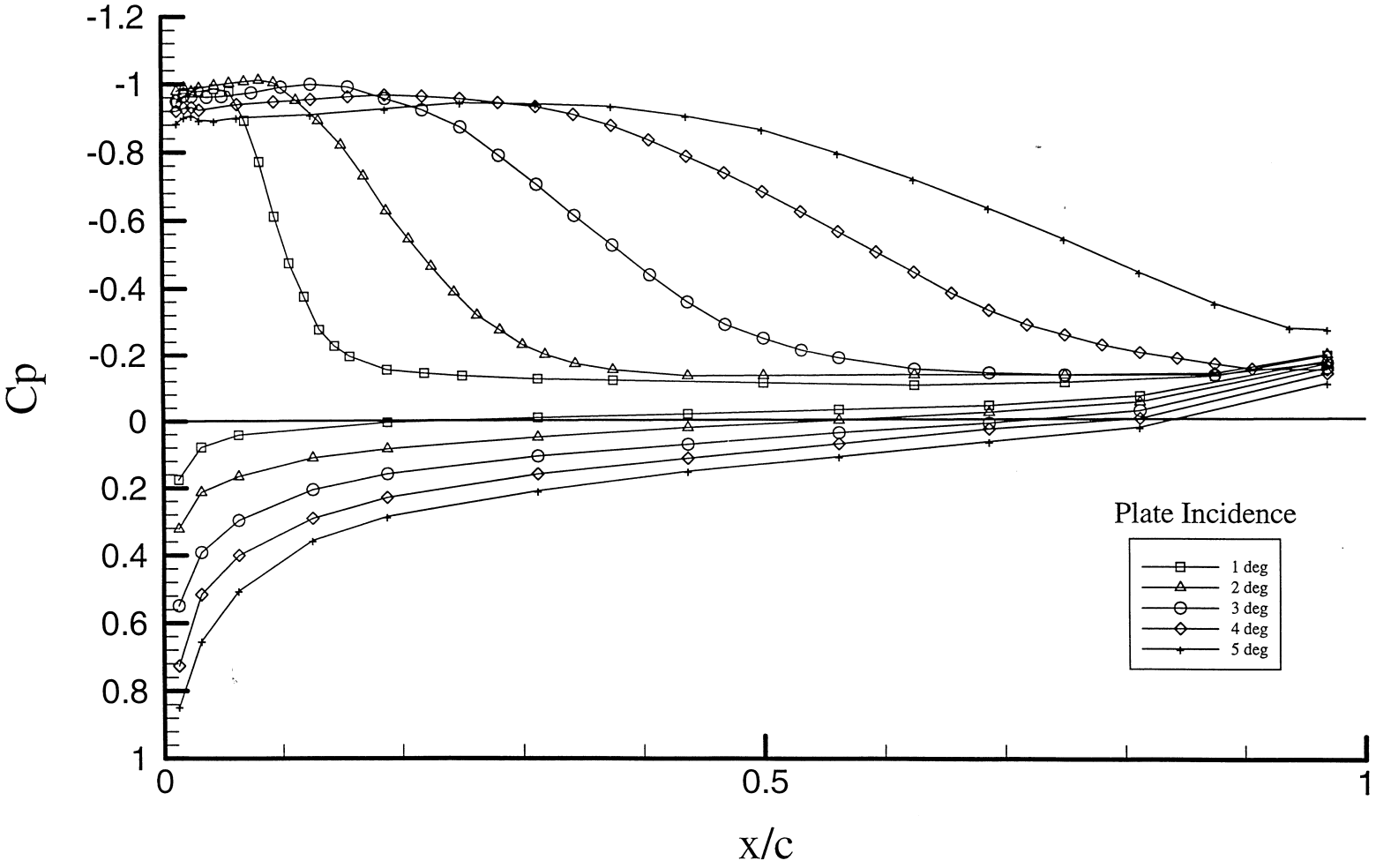

Fig. 5 Distribution of the static pressure coefficient for various angles of incidence: $U_\infty = 20\,\text{m/s}$, $Re_c = 2.13 \times 10^5$

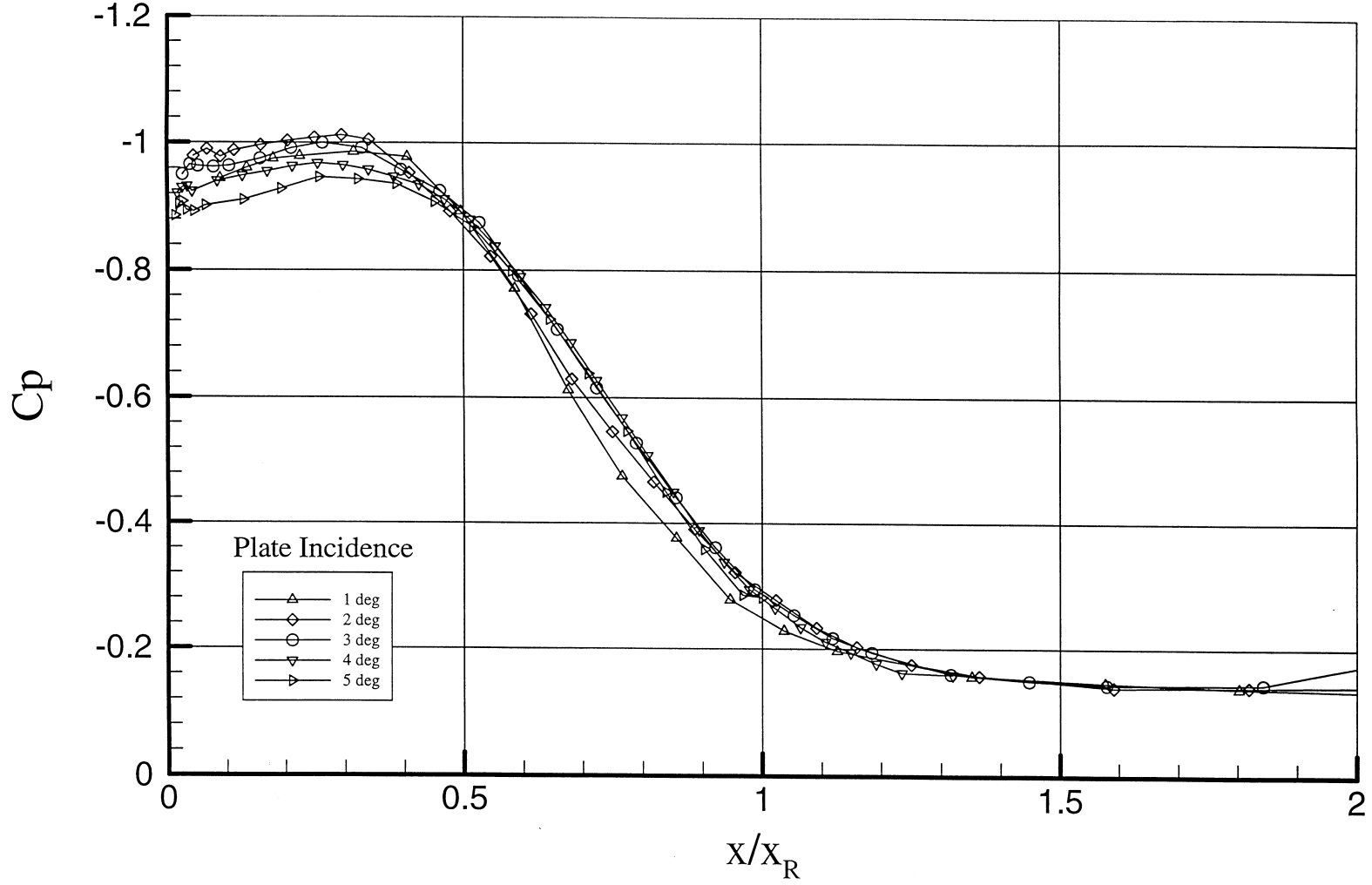

Fig. 6 Distribution of the static pressure coefficient, non-dimensionalized to the reattachment length for various angles of incidence: $U_\infty = 20\,\text{m/s}$, $Re_c = 2.13 \times 10^5$

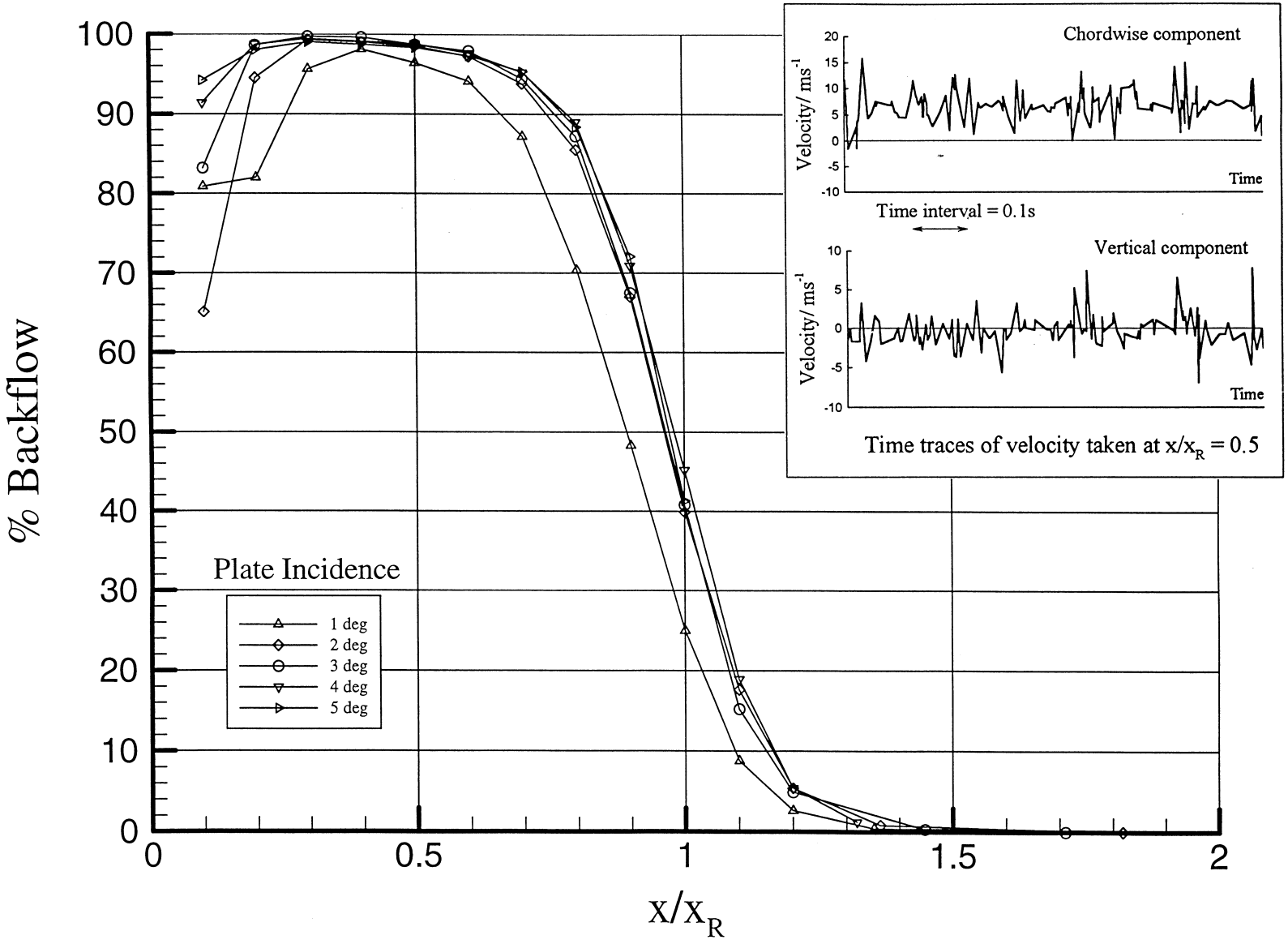

Fig. 7 Intermittency in the reverse flow region for various angles of incidence: $U_\infty = 20\,\text{m/s}$, $Re_c = 2.13 \times 10^5$ and $y = 0.5\,\text{mm}$

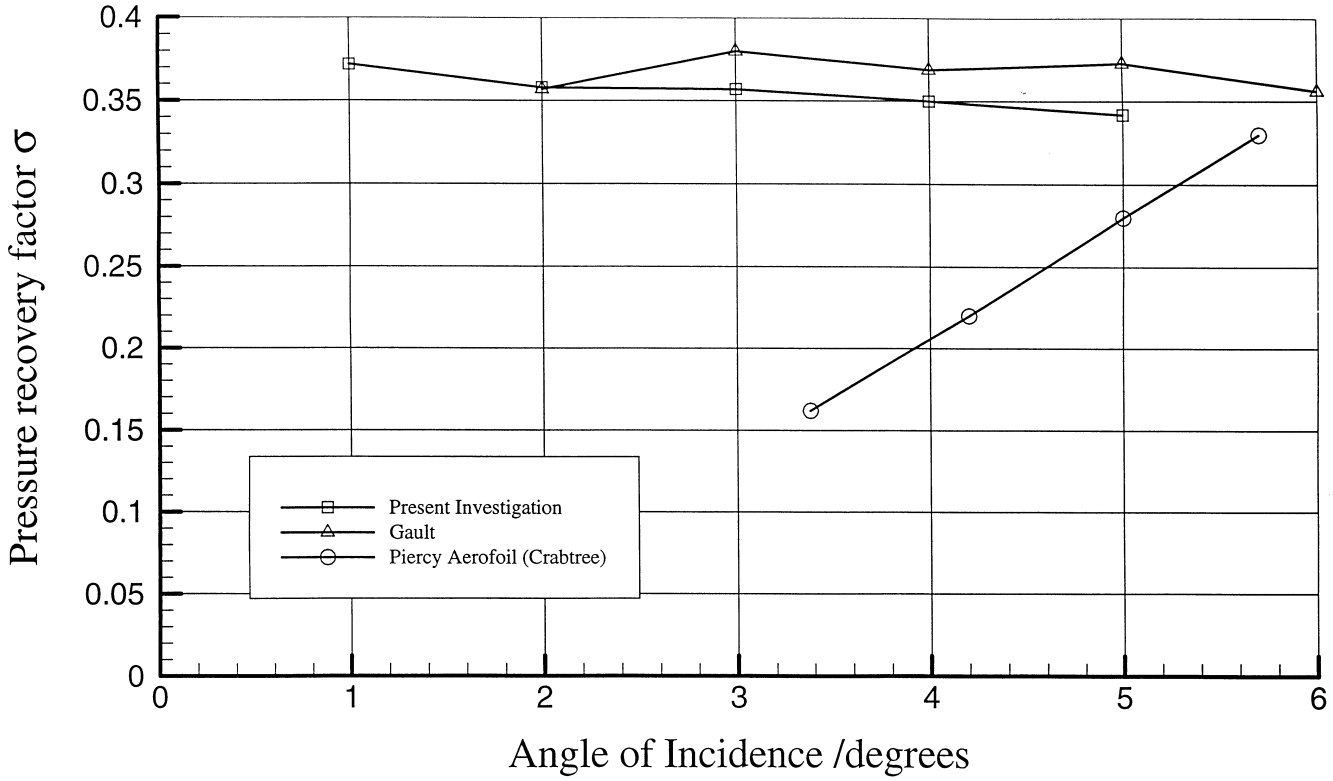

Fig. 8 Pressure recovery factor for long and short bubbles

as close to the leading edge as could be resolved by detailed small-scale surveys. The nature of a stagnation point means that it must be balanced by equal pressures to either side to be stable. It cannot therefore exist on an infinitely sharp leading edge unless at zero incidence. Although the leading edge appears to be sharp, it clearly must have thickness and be somewhat rounded. This enables a pressure balance for the stagnation point to exist and explains why there is no apparent movement through the first 20° incidence. The consequence is that there is no significant boundary layer developed from the stagnation point around the leading edge before separation occurs on the upper surface.

3.4 Structure of the separation bubble close to the leading edge

The flow close to the leading edge is important in determining the nature of the flowfield over the rest of the plate. Figure 10 shows the chordwise r.m.s. velocity close to the leading edge for both high and low Reynolds numbers, i.e. 0.53×10^5 and 2.13×10^5. It can be seen that the spreading rate of the shear layer is greater at the lower Reynolds number, analogous to the effect that Reynolds number has on the thickening of a normal attached boundary layer. The onset of transition, however, occurs at about the same position in both cases, as seen by the plots of chordwise r.m.s. velocity along the centre-line of the shear layer in Fig. 11. Thus, the influence of the shear layer will reach the surface in a shorter distance at low Reynolds number and might therefore be expected to initiate reattachment sooner. Further assessment of the dependence of the bubble length on Reynolds number is made in a later section.

The separation of the flow at the leading edge will always initiate a laminar shear layer, which previous workers and the present study show to undergo rapid transition. For example, Newman and Tse [**4**] found that transition occurred at a Reynolds number based on a shear layer width of the order of 100 which was very close to the leading edge. Similarly, Gault [**11**] found that the extent of the laminar flow was virtually zero in tests at a chord Reynolds number of 4×10^6. The early transition compared with that of the short bubble suggests that some form of initial instability is affecting the shear layer close to the leading edge in the flat plate case. This must be the result of the severe shear generated by the sharp edge separation.

The stabilization of the reverse flow in the bubble adjacent to the surface has already been discussed, and this feature assists the formation of the secondary separation bubble. It reduces the velocity gradient adjacent to the surface, leaving the reverse boundary layer susceptible to separation in the adverse pressure gradient occurring over the front half of the bubble. The secondary bubble rotates in the opposite direction to the main bubble and reattaches close to the leading edge in the

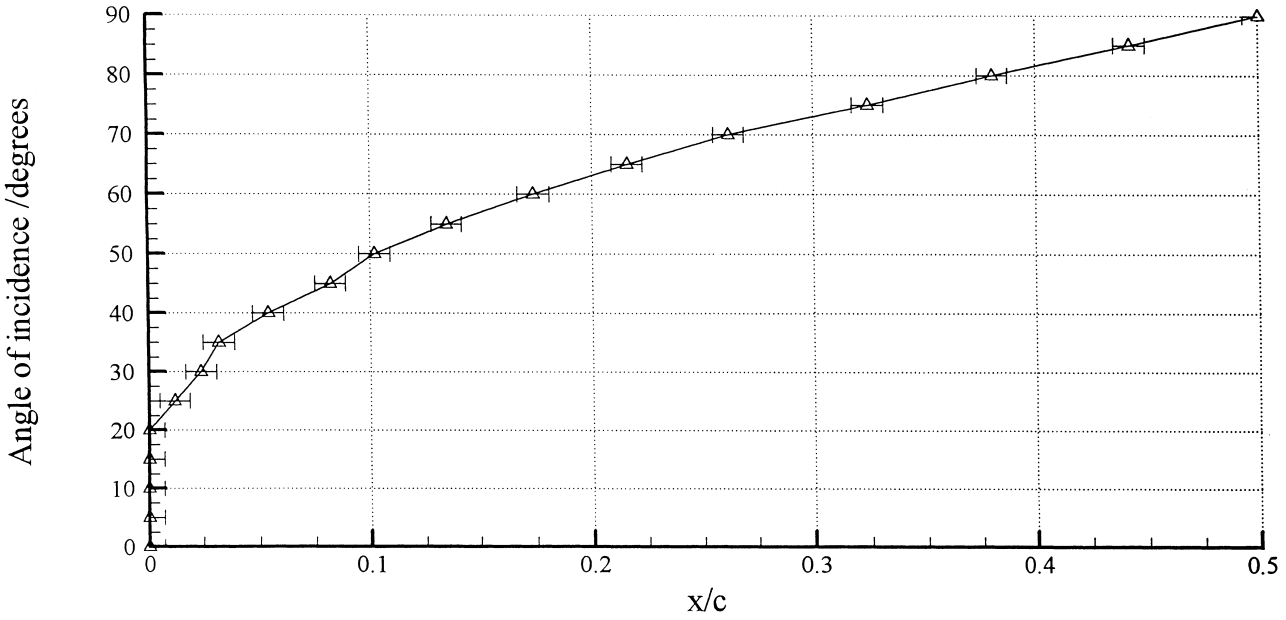

Fig. 9 Location of the forward stagnation point for various angles of incidence: $U_\infty = 4\,\text{m/s}$, $Re_c = 0.2 \times 10^5$

strong chordwise favourable pressure gradient that occurs there.

Figure 12 shows chordwise velocity profiles through the secondary separation bubble. It can be seen that the maximum velocity near the surface is only about 4 per cent of U_∞. The length of this bubble varies between 2 and 8 per cent chord over the range of incidences and Reynolds numbers investigated. A major effect of the secondary separation bubble is to enhance the main shear layer immediately after leading edge separation owing to the opposing velocity on its inner side. This increases the velocity gradient in the shear layer, with consequent influence on transition. The driving force for the secondary separation bubble is therefore not the main shear layer, which opposes its rotation, but entrainment at the separation of the reverse flow, together with the chordwise pressure gradient near the leading edge.

3.5 Effect of Reynolds number variation on the flow structure

Looking firstly at the secondary bubble, Fig. 13 shows that its length decreases progressively as the Reynolds number is increased. This is because increasing the Reynolds number causes the reverse flow boundary layer to adopt a more turbulent profile and thus become more resistant to separation in the forward adverse pressure gradient region.

The length of the primary separation bubble is expected to be only weakly dependent on Reynolds number because the reattachment process is an entirely turbulent one. Figure 14 shows this to be largely the case, for a range of incidences and for two different chord lengths. However, some variation does occur as the Reynolds number is increased. The reattachment length first decreases then rises again, up to a certain limit above which any further change in the Reynolds number has a negligible effect. This limit was around 10^5, increasing slightly as incidence was reduced because, at lower incidence, the bubble is much shallower and hence viscous effects will be intensified. In similar experiments, Newman and Tse [**4**] found that the reattachment length became independent of the Reynolds number above about 2.5×10^5. In other types of long bubble flows such as the experiments of Castro and Haque [**1**] and Ruderich and Fernholz [**19**], similar limits on the effect of the Reynolds number were found.

The level of entrainment in the shear layer determines the magnitude of the reverse flow velocities, hence controlling the static pressures at the surface and the curvature of the dividing streamline towards reattachment. At low Reynolds numbers, entrainment is low and therefore the reattachment length is high, assuming reattachment occurs at all. Initially, as the Reynolds number is increased, entrainment also increases and the bubble shortens until a minimum length is reached at which entrainment has reached its maximum; i.e. the shear layer is effectively fully turbulent. Beyond this, the lateral contraction of the shear layer causes reattachment to

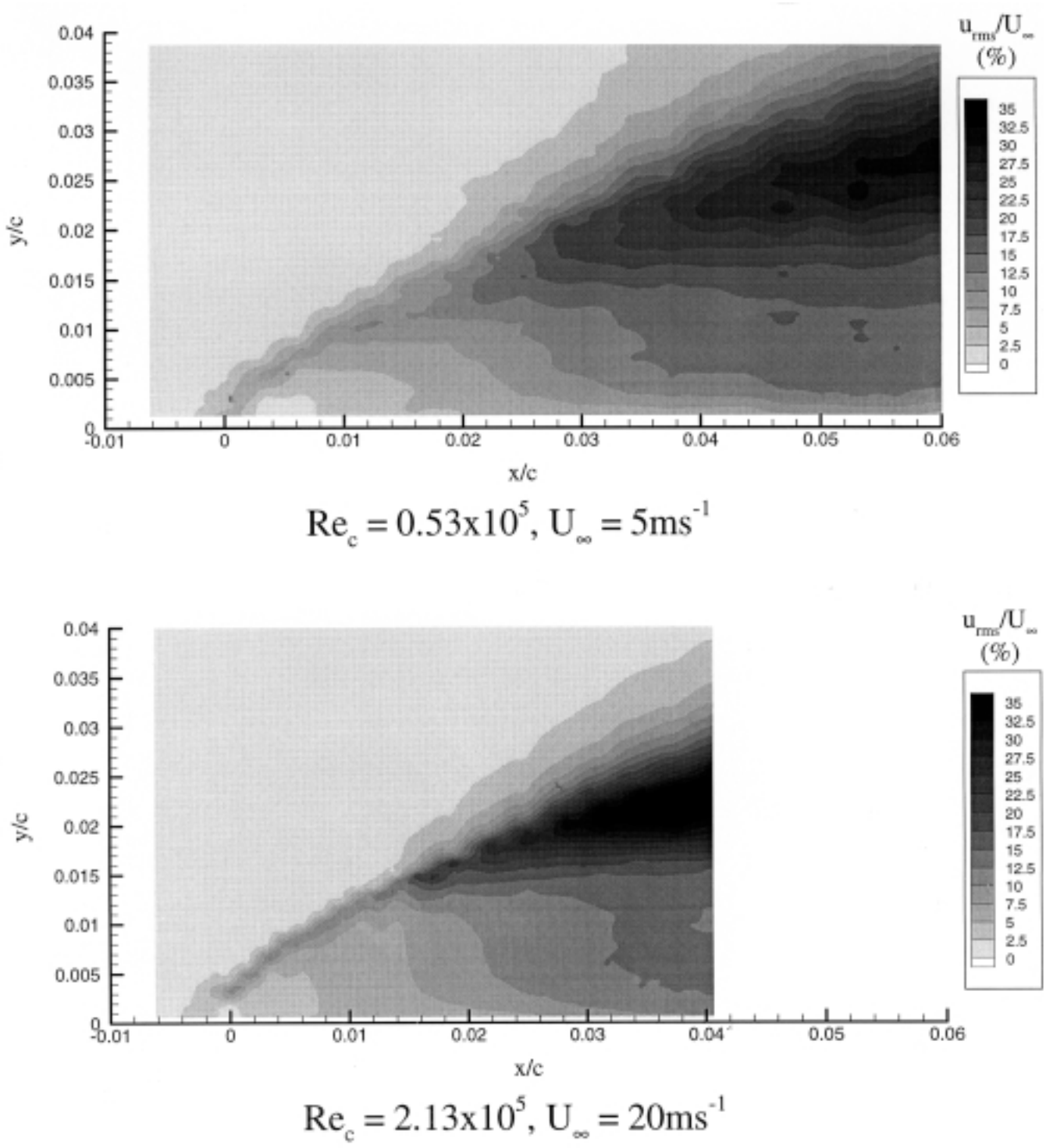

Fig. 10 Effect of the Reynolds number on the distribution of $u_{\text{r.m.s.}}/U_\infty$ near the leading edge for $\alpha = 3^\circ$

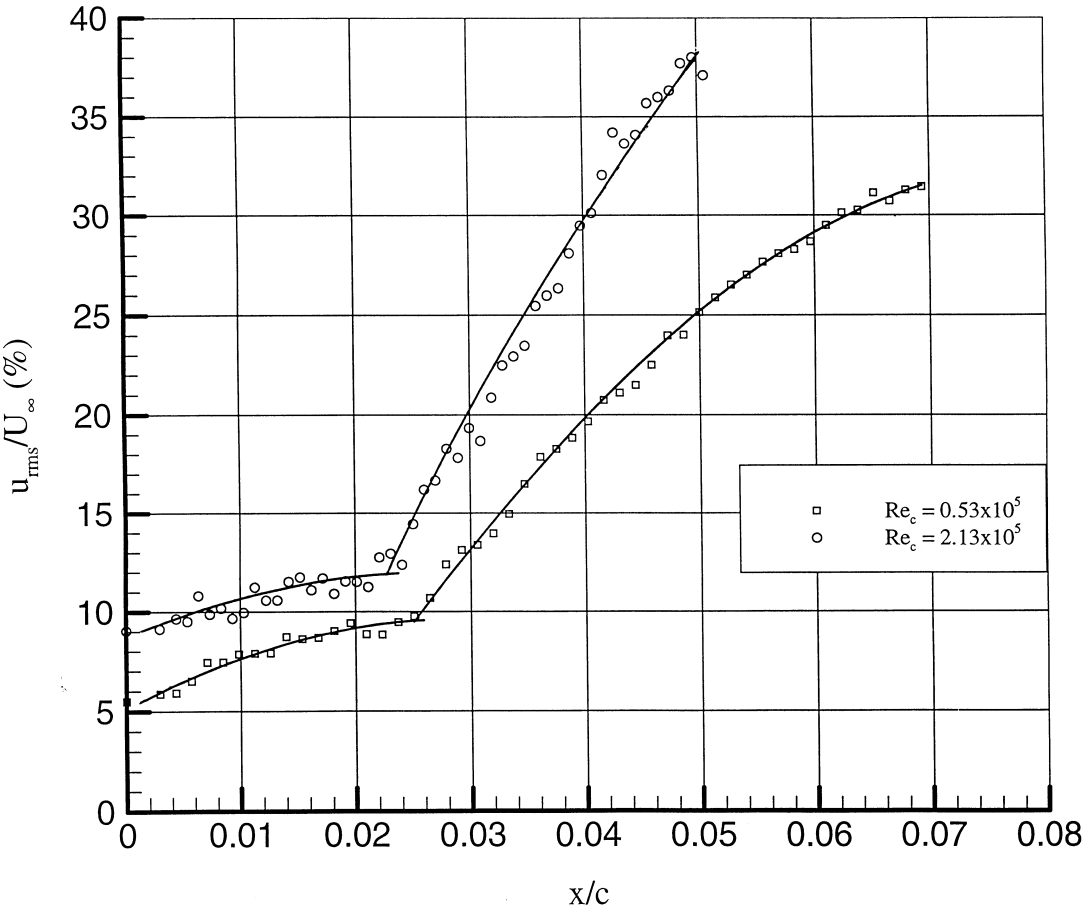

Fig. 11 Variation in $u_{\text{r.m.s.}}/U_\infty$ with distance along the shear layer for $\alpha = 3°$

be delayed, as described earlier in relation to Fig. 10. Eventually, the reduction in lateral growth rate become negligible and the reattachment length then remains constant for further increase in the Reynolds number.

4 CONCLUSIONS

With the aid of advanced laser anemometry techniques, the structure of a separation bubble behind a sharp leading edge has been investigated in detail. This has shed new light on the mechanisms associated with the process of bubble development and reattachment. A small secondary separation bubble has been found adjacent to the leading edge, which is thought to have an important influence on the main bubble structure.

A key feature of the flow is the entrainment on the low-velocity edge of the shear layer which is responsible for the reverse flow inside the bubble, the form of the pressure distribution and the curvature of the shear layer. The degree of entrainment is determined by the Reynolds number of the flow, with the length of the main separation bubble being primarily dependent on incidence but showing a variation with Reynolds number below about 10^5.

In the reverse flow boundary layer, evidence was found of periodic stabilization due to the favourable pressure gradient over the rear half of the bubble. Ahead of this, the boundary layer is decelerated by an adverse pressure gradient which leaves it more susceptible to separation close to the leading edge.

The reattachment region is highly unstable owing to imbalances between the quantity of fluid entrained by the shear layer and that returned by the reverse flow region. Downstream of reattachment, the boundary layer rapidly changes form towards that of a normal turbulent boundary layer profile owing to the injection of high-velocity fluid into the lower portion of the layer and a reduction in the turbulence intensity.

Separation bubbles of different sizes have been shown to exhibit similarities in the chordwise static pressure profiles and in the intermittency of the reverse flow region, when these quantities are non-dimensionalized with respect to the reattachment length of the bubble. Although small in size (2–8 per cent chord), the secondary separation bubble has the effect of increasing the velocity gradient in the shear layer close to the leading

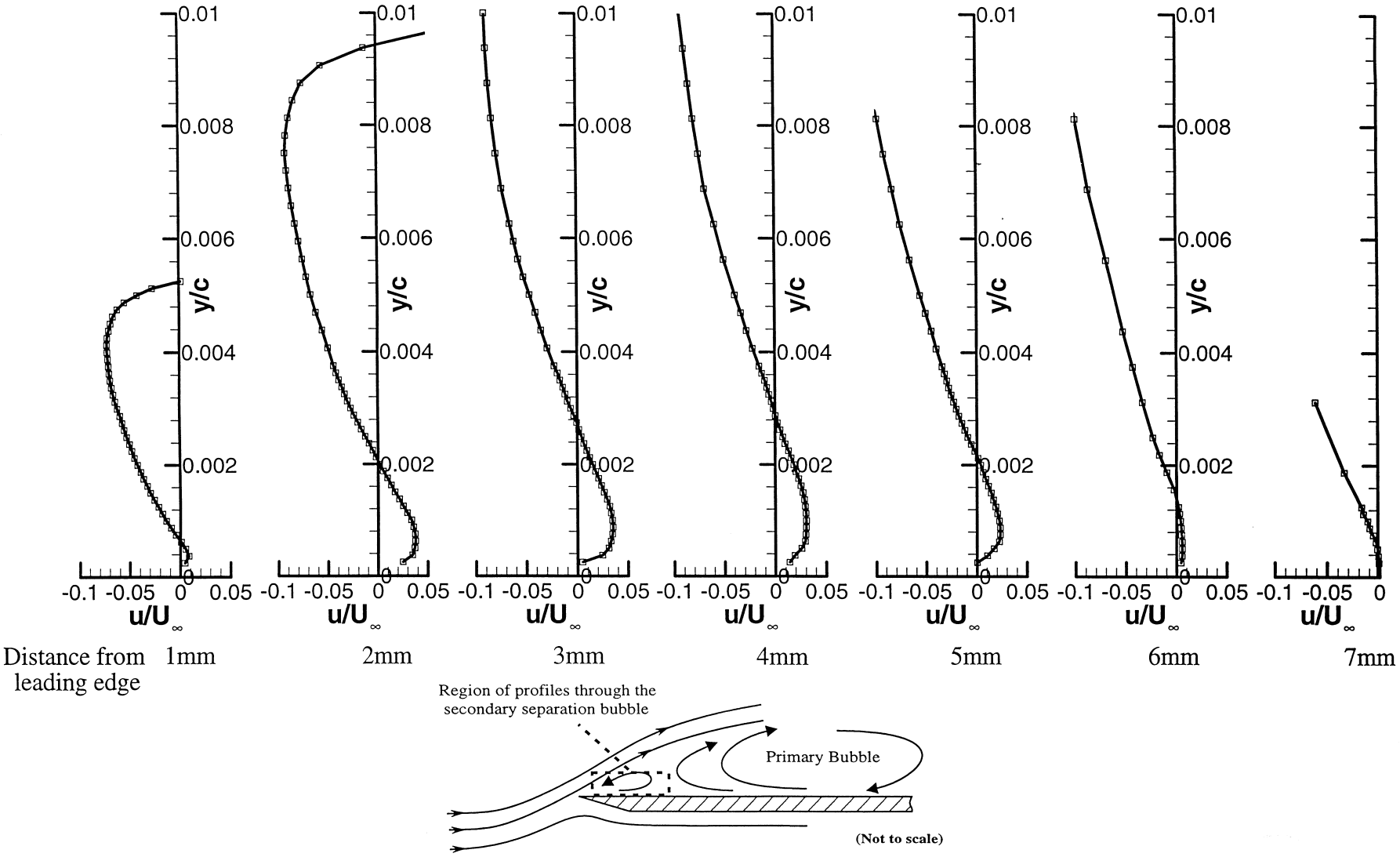

Fig. 12 Mean chordwise velocity distributions normal to the plate through the secondary separation bubble: $\alpha = 3^\circ$, $U_\infty = 20\,\text{m/s}$ and $Re_c = 2.13 \times 10^5$

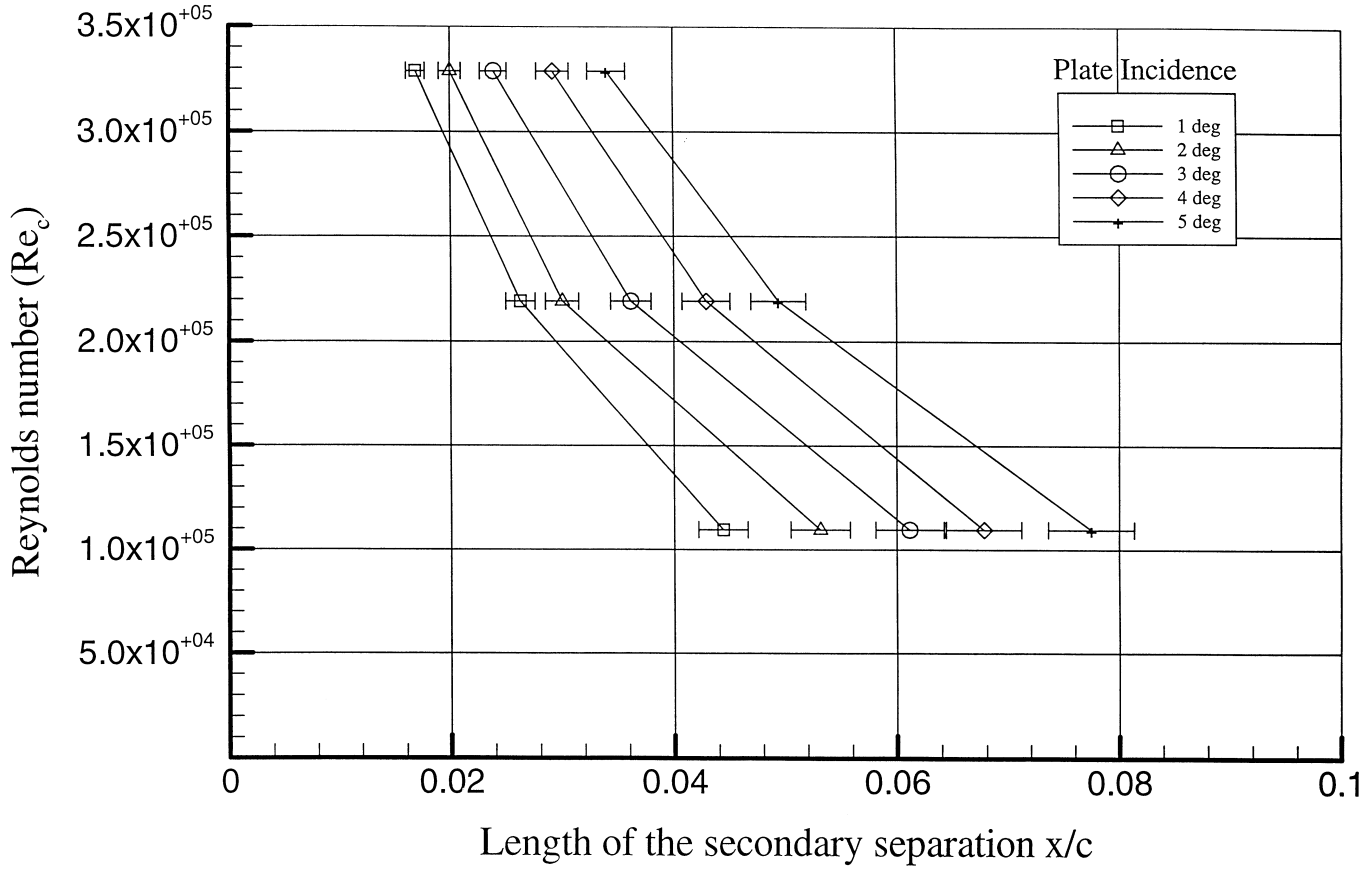

Fig. 13 Reynolds number dependence of the secondary separation bubble length for various angles of incidence

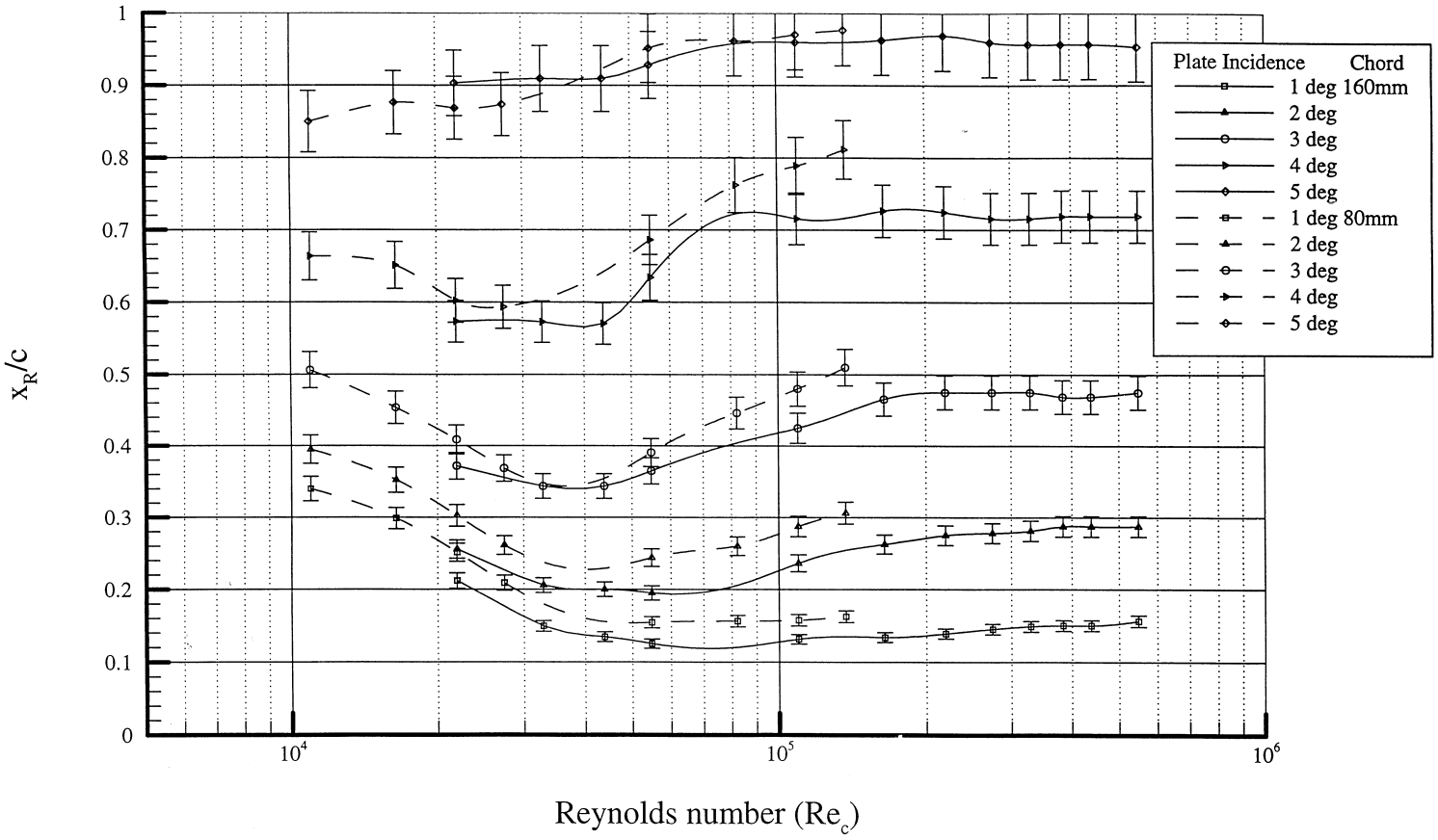

Fig. 14 Variation in reattachment length with Reynolds number for various angles of incidence and two different plate chords

edge, which encourages the shear layer to undergo early transition. The length of this bubble is dependent on the Reynolds number even when the length of the primary bubble has become insensitive to that parameter. The stagnation point has been shown to remain attached to the leading edge over and beyond the incidence range for which the separation bubble exists.

The results provide a detailed test case to assist in the validation of numerical calculations of thin aerofoil flows. Jackson and Fiddes [**2**] had identified that such a test case was not available from previous work but was very necessary for further progress in the analysis of this flow regime. In addition, the understanding of the main characteristics of the separation bubble that has now been provided should aid design processes where the minimization of such bubbles is required.

REFERENCES

1 **Castro, I. P.** and **Haque, A.** The structure of a turbulent shear layer bounding a separation region. *J. Fluid Mechanics*, 1987, **179,** 439–468.

2 **Jackson, P. S.** and **Fiddes, S. P.** Two-dimensional flow past flexible sail sections close to ideal incidence. *Aeronaut. J.*, 1995, **99,** 217–225.

3 **Barrett, R. V.** Design and performance of a new low turbulence wind tunnel at Bristol University. *Aeronaut. J.*, 1984, **88,** 86–90.

4 **Newman, B. G.** and **Tse, M-C.** Incompressible flow past a flat plate aerofoil with leading edge separation bubble. *Aeronaut. J.*, 1992, **96,** 57–64.

5 **Barrett, R. V.** and **Swales, C.** Realisation of the full potential of the laser Doppler anemometer in the analysis of complex flows. *Aeronaut. J.*, 1998, **102,** 313–320.

6 **MacManus, D., Eaton, J., Barrett, R. V., Rickards, J.** and **Swales, C.** Mapping the flow field induced by a HLFC perforation using a high resolution LDV. In Proceedings of 34th Aerospace Sciences Meeting and Exhibition, Reno, Nevada, January 1996, AIAA 96-0097.

7 **Melling, A.** and **Whitelaw, J. H.** Seeding of gas flows for laser anemometry. *DISA Informn*, 1973, (15), 5–14.

8 **Pfeifer, H. J.** Post processing of data. In *VKI Lecture Series—Laser Velocimetry*, Rhode Saint Genese, Belgium, June 1991.

9 **McLaughlin, D. K.** and **Tiedermann, W. G.** Biasing corrections for individual realisation of laser anemometer measurements in turbulent flows. *Phys. Fluids*, 1973, **16**(12), 2082–2088.

10 **Bradshaw, P.** and **Wong, F. Y. F.** Reattachment of a turbulent shear layer. *J. Fluid Mechanics*, 1972, **52,** 113–135.

11 **Gault, D. E.** An investigation at low speed of the flow over a simulated flat plate at small angles of attack using pitot static and hot-wire probes. NACA TN-3876, 1957.

12 **Horton, H. P.** A semi-empirical theory for the growth and bursting of laminar separation bubbles. CP-1073, Aeronautical Research Council, London, 1967.

13 **Schmidt, G. S.** and **Mueller, T. J.** Analysis of low Reynolds number separation bubbles using semiempirical methods. *Am. Inst. Aeronaut. Astronaut. J.*, 1989, **27**(8), 993–1001.

14 **O'Meara, M. M.** An experimental investigation of the separation bubble flow field over an airfoil at low Reynolds numbers. MS thesis, University of Notre Dame, Notre Dame, Indiana, 1985.

15 **Simpson, R. L., Chew, Y-T.** and **Shivaprasad, B. G.** The structure of a separating turbulent boundary layer. *J. Fluid Mechanics*, 1981, **113,** 23–90.

16 **Westphal, R. V., Eaton, J. K.** and **Johnston, J. P.** Experimental study of flow reattachment in a single sided sudden expansion. NASA CR-3765, 1984.

17 **Crabtree, L. F.** The formation of regions of separated flow on wing surfaces. R&M-3122, Aeronautical Research Council, London, 1957.

18 **Gaster, M.** The structure and behaviour of laminar separation bubbles. AGARD CP-4 Part 2, 1966, pp. 813–854.

19 **Ruderich, R.** and **Fernholz, H. H.** An experimental investigation of a turbulent shear layer with separation, reverse flow and reattachment. *J. Fluid Mechanics*, 1986, **163,** 283–322.

